JACS
JOURNAL OF THE AMERICAN CHEMICAL SOCIETY

Subscriber access provided by University of Massachusetts Amherst Libraries

Communication

Grain-Boundary-Rich Copper for Efficient Solar-Driven Electrochemical CO2 Reduction to Ethylene and Ethanol

ZHIQIANG CHEN, Tuo Wang, Bin Liu, Dongfang Cheng, Congling Hu, Gong Zhang, Wenjin Zhu, Huaiyuan Wang, Zhi-Jian Zhao, and Jinlong Gong

J. Am. Chem. Soc., **Just Accepted Manuscript** • DOI: 10.1021/jacs.0c00971 • Publication Date (Web): 27 Mar 2020

Downloaded from pubs.acs.org on March 27, 2020

Just Accepted

"Just Accepted" manuscripts have been peer-reviewed and accepted for publication. They are posted online prior to technical editing, formatting for publication and author proofing. The American Chemical Society provides "Just Accepted" as a service to the research community to expedite the dissemination of scientific material as soon as possible after acceptance. "Just Accepted" manuscripts appear in full in PDF format accompanied by an HTML abstract. "Just Accepted" manuscripts have been fully peer reviewed, but should not be considered the official version of record. They are citable by the Digital Object Identifier (DOI®). "Just Accepted" is an optional service offered to authors. Therefore, the "Just Accepted" Web site may not include all articles that will be published in the journal. After a manuscript is technically edited and formatted, it will be removed from the "Just Accepted" Web site and published as an ASAP article. Note that technical editing may introduce minor changes to the manuscript text and/or graphics which could affect content, and all legal disclaimers and ethical guidelines that apply to the journal pertain. ACS cannot be held responsible for errors or consequences arising from the use of information contained in these "Just Accepted" manuscripts.

is published by the American Chemical Society. 1155 Sixteenth Street N.W., Washington, DC 20036

Published by American Chemical Society. Copyright © American Chemical Society. However, no copyright claim is made to original U.S. Government works, or works produced by employees of any Commonwealth realm Crown government in the course of their duties.

Grain-Boundary-Rich Copper for Efficient Solar-Driven Electrochemical CO_2 Reduction to Ethylene and Ethanol

Zhiqiang Chen, Tuo Wang, Bin Liu, Dongfang Cheng, Congling Hu, Gong Zhang, Wenjin Zhu, Huaiyuan Wang, Zhi-Jian Zhao, and Jinlong Gong*

School of Chemical Engineering and Technology, Tianjin University; Key Laboratory for Green Chemical Technology of Ministry of Education, Tianjin University; Collaborative Innovation Center of Chemical Science and Engineering (Tianjin), Tianjin 300072, China

Supporting Information Placeholder

ABSTRACT: The grain boundary in copper-based electrocatalysts has been demonstrated to improve the selectivity of solar-driven electrochemical CO_2 reduction towards multi-carbon products. However, the approach to form grain boundaries in copper is still limited. This paper describes a controllable grain growth of copper electrodeposition via poly (vinylpyrrolidone) used as an additive. A grain-boundary-rich metallic copper could be obtained to convert CO_2 into ethylene and ethanol with a high selectivity of 70% over a wide potential range. In-situ attenuated total reflection surface-enhanced infrared absorption spectroscopy unveils that the existence of grain boundaries enhances the adsorption of the key intermediate (*CO) on the copper surface to boost the further CO_2 reduction. When coupling with a commercially available Si solar cell, the device achieves a remarkable solar-to-C2-products conversion efficiency of 3.88% at a large current density of 52 $mA{\cdot}cm^{-2}$. This low-cost and efficient device is promising for large-scale application of solar-driven CO_2 reduction.

The electrochemical transformation of CO_2 to value-added multi-carbon (C2+) products is a potential solution to close the anthropogenic carbon cycle, which could be driven by renewable energies such as solar power.[1-2] Copper is a unique metal that can reduce CO_2 to C2+ products.[3-6] However, the moderate binding energy of copper leads to poor product selectivities.[7] It is believed that grain boundary (GB) can control the product selectivity of CO_2 reduction reaction (CO_2RR).[8-9] The density of GBs of copper exhibits a quantitative correlation with CO reduction reaction activity.[10] Therefore, GBs are considered as one of the reasons for the increased selectivity of oxide-derived copper towards C2+ products.[11-13] But the reduction of the copper oxide would lead to the change of copper valence states, [14] making it difficult to identify the role of GBs. Thus, new approaches are desired to introduce GBs into metallic copper without changing the valence states of copper.

This communication describes the fabrication of a grain-boundary-rich copper catalyst (GB-Cu) by the additive-control electrodeposition, in which poly(vinylpyrrolidone) (PVP) is used as an additive. Unlike other additives such as citric acid that forms complex with Cu ion to control the deposition kinetics, PVP is a physicochemically inert polymer, which can adsorb on copper surface reversibly to kinetically increase the rate of nucleation and reduce the size of crystallite.[15-18] Moreover, the inert nature of PVP avoids the introduction of carbon contamination. With the existence of GBs, GB-Cu shows a remarkable FE of about 70% for C2 products in the wide potential range, which achieves a solar-to-C2 energy conversion efficiency of 3.88 % with a remarkable current density of 52 $mA{\cdot}cm^{-2}$ when coupled to a Si solar cell. In-situ attenuated total reflection surface-enhanced infrared absorption spectroscopy (ATR-SEIRAS) investigations and theoretical calculations are adopted to explore the role of GBs of copper during CO_2RR.

The copper catalysts were in-situ grown on gas diffusion layer by potentiostatic electrodeposition with or without PVP (details in Supporting Information). As shown in scanning electron microscopy (SEM) images, the surface of GB-Cu is piled up by tiny particles, which is different form ED-Cu (Figure S1). Transmission electron microscopy (TEM) reveals that the copper electrodeposited without PVP (denoted as ED-Cu) shows a uniform lattice orientation without GBs (Figure 1a). When adding PVP as the additive, a high density of grain boundaries is introduced into GB-Cu nanoparticle (Figure 1b, more images of different GB-Cu in Figure S2). The lattice spacing of ED-Cu and GB-Cu nanoparticles (Figure 1a and b) both correspond to (111) facet of copper, which is consistent with the X-ray diffraction (XRD) result (Figure 1c). GB-Cu and ED-Cu both present a sharp Cu 2p peak at 932.4 eV in X-ray photoelectron spectroscopy (XPS) (Figure 1d), corresponding to Cu^0 or Cu^+ species.[19] Auger electron spectroscopy (AES) of Cu LMM (Figure S3) illustrates that GB-Cu mainly consists of Cu^0 (918.6 eV), with a very limited amount of Cu^+ (916.6 eV), which could be caused by the rapid oxidation in the air.[20-21] These results indicate that PVP makes no noticeable influence on the exposed crystal planes and chemical states of copper during the electrodeposition while inducing the formation of GBs in copper.

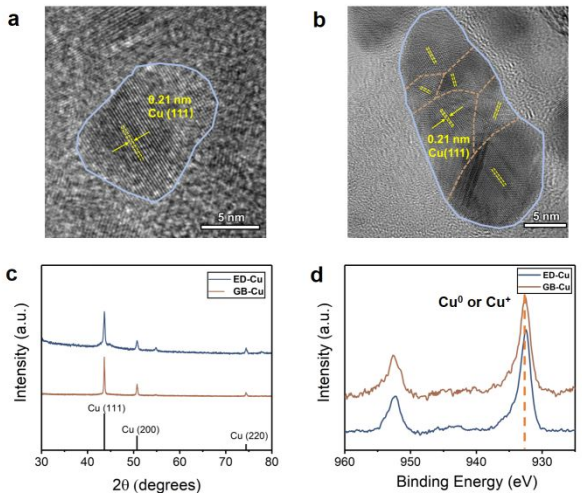

Figure 1. HRTEM images of (a) ED-Cu catalysts and (b) GB-Cu catalysts. Different lattice orientation regions divided by orange dotted lines; (c) XRD and (d) Cu 2p XPS spectra of as-prepared ED-Cu and GB-Cu catalysts.

For electrochemical measurement, the CO_2 electroreduction reaction was conducted in a three-compartment flow cell (Figure S4). Linear sweep voltammetry (LSV) shows that ED-Cu and GB-Cu exhibit similar electrocatalytic activity (Figure S5). However, GB-Cu shows a higher selectivity for ethylene (~38 % at –1.2 V *vs.* RHE) and much less hydrogen production than ED-Cu (Figure 2a and b). Combined with liquid-phase products, the Faradaic efficiency for C2+ products of GB-Cu (Figure 2c) including ethylene, ethanol, and propanol reaches 73 % in a wide potential range from –1.0 to –1.3 V *vs.* RHE, which is superior to most of the metallic copper electrocatalysts (Table S1). Compared with ED-Cu, GB-Cu shows a much higher selectivity for C2 products at each applied potential (Figure 4d).

Moreover, the ethanol-to-ethylene ratio is enhanced from 0.49 on ED-Cu to 0.85 on GB-Cu (Figure S6). The ethanol FE of GB-Cu achieves 31.74 % with a current density of 45 mA·cm^{-2} at –1.3 V *vs.* RHE (Figure S7), which is superior to most previously reported Cu-based electrocatalysts (Table S2). It has been identified that ethylene and ethanol are produced at different active sites of copper by the isotope-labeling method,[22] while the undercoordinated sites, such as GBs, are more favorable for the formation of oxygenates.[23] In this respect, the higher ethanol-to-ethylene ratio on GB-Cu compared with ED-Cu could be a good indication that GBs play a significant role in the product distribution of CO_2RR.

To ensure that the improved CO_2RR performance for C2 products is indeed originated from the introduction of GBs, the effect of PVP and surface area should be excluded. The characteristic Fourier transform infrared spectroscopy (FTIR) bands of PVP, such as C–N (stretching at 1292 cm^{-1}) and C–O (vibrating at 1679 cm^{-1}) as shown in PVP reagent,[24] cannot be observed for GB-Cu (Figure S8), revealing the absence of PVP on GB-Cu. Though PVP will not participate in CO2RR, it can alter the C2 products selectivity by inducing the formation of GB (details in Figure S9). In addition, the similar ECSA (Figure S10 and Table S3) of GB-Cu and ED-Cu indicates that the higher catalytic activity of GB-Cu is not caused by the increase of surface area, but the improvement related to intrinsic active sites.

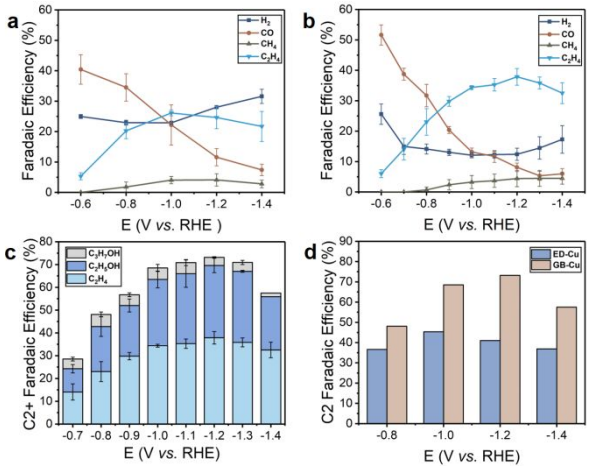

Figure 2. Faradaic efficiencies of gas products on (a) ED-Cu and (b) GB-Cu as a function of the electrode potential; (c) Faradaic efficiencies of C2+ products on GB-Cu; (d) Comparison of Faradaic efficiencies of C2 products on ED-Cu and GB-Cu.

To explore the impact of the GB formation on the CO_2 reduction, in-situ ATR-SEIRAS was employed to monitor the CO adsorption behavior in CO-saturated KOH electrolyte. The absorption band at 1650 cm^{-1} is corresponding to the H–O–H bending vibration of water (Figure S11).[25] On the surface of ED-Cu, there is a stretching band at 2070 cm^{-1} at low potential (Figure 3a), corresponding to the stretching band of linearly atop-bound CO (CO_{ad}) (1920 ~ 2100 cm^{-1}) on Cu surface.[26-27] As for GB-Cu, the CO_{ad} band presents a distinct red-shift from 2070 cm^{-1} to 2060 cm^{-1} at –0.1 V *vs.* RHE (Figure 3b). The lower wavenumber of the CO_{ad} band indicates the stronger adsorption of CO on the GB-Cu surface.[28-31] As shown above, both of ED-Cu and GB-Cu expose the same (111) plane of metallic copper with similar nanoparticle morphology. The main difference between ED-Cu and GB-Cu is the formation of GBs on GB-Cu, which should be attributed to explain the enhancement of CO adsorption.

Meanwhile, the adsorption of CO on GB-Cu at different potentials is different from ED-Cu. Until the applied potential reaches –0.4 V *vs.* RHE, the peak areas of the CO_{ad} band region of GB-Cu is increasing indicating the increased coverage of CO_{ad} on GB-Cu surface (Figure S12), which is proportional to the surface coverage of CO.[32-33] Moreover, the distinct CO_{ad} bands are still observed on the GB-Cu surface under much more negative potentials until –1.0 V *vs.* RHE, while the CO_{ad} bands on the ED-Cu are absent after –0.5 V *vs.* RHE. Under the same cathodic potentials, the relationship between applied potential and CO adsorption, such as the Stark effect and π-interaction, should be similar.[29] Hence, it can be proposed that GBs of GB-Cu could enhance and stabilize CO adsorption at much more negative potentials.

Density functional theory (DFT) calculations are employed to further reveal the role of GB on the high selectivity towards C2 production. The Σ3 twin boundary, which presents the highest density of coincident lattice sites at the GB plane, is chosen for its stable atomic structure[34]. The calculation of CO binding energies in different sites (Figure

3c-3d) suggests that CO is binding stronger in both convex GB sites (GB1) and concave GB sites (GB2) than terrace sites (t1~t7), consisting with the results of in-situ ATR-SEIRAS. It is worth noting that the GBs also alter the coordination of their surrounding atoms, therefore slightly increasing the CO binding energies of t1, t2 and t7 sites than other terrace sites. The increasing CO binding energy at the GBs is beneficial to the kinetics of CO dimerization.

As for the C–C coupling step, many studies have shown that CO dimerization is the first step towards C2 products, followed by the hydrogenation of *COCO to form *COCHO[35-37]. Bell *et al* found that *COCHO was a critical intermediate towards C2 products. [38] The pathway to ethylene or ethanol is downhill thermodynamically from *COCHO intermediate.[39] Hence, the formation energy of *COCHO is an appropriate descriptor to describe the C–C coupling step. From our calculations, the formation energy of *COCHO intermediate is 0.46 eV on GB1 site and 0.58 eV on GB2 site, 0.24 eV and 0.12 eV lower than terrace site like t4 (0.70 eV), respectively (Figure S13), suggesting that the presence of GB can promote the C–C coupling.

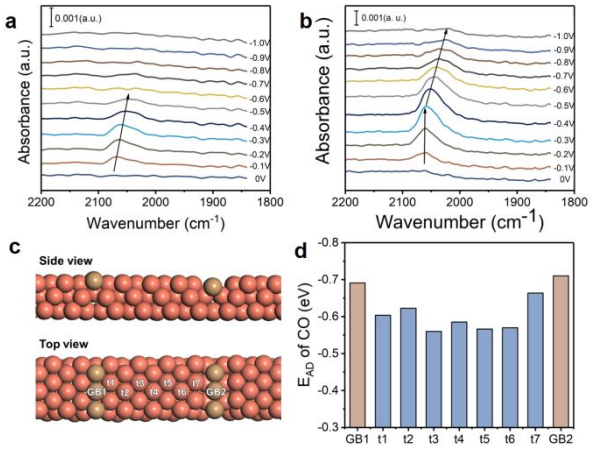

Figure 3. In-situ ATR-SEIRAS spectras of (a) ED-Cu and (b) GB-Cu; (c) Different binding sites on the schemed atomic structure of GB-Cu; (d) *CO binding energies in different sites of the schemed structure of GB-Cu.

As mentioned above, GB-Cu keeps a high selectivity for C2 products in a wide potential range, showing a tremendous potential to be the cathode for a photovoltaic-electrochemical (PV-EC) system. As for the anode, a low-cost OER anode electrocatalyst, Se-(NiCo)S_x/$(OH)_x$ nanosheets, was adopted as reported before.[40] The onset voltage of the cell, defined by the difference between the onset potentials (defined as the potential required to achieve an absolute current density of 1 mA·cm^{-2}) of cathode and anode, is 1.8 V when the Ni foam is used as the anode (Figure 4a). When using the Se-(NiCo)S_x/$(OH)_x$ nanosheets as the anode, the onset voltage is reduced to 1.5 V (Figure 4b).

According to the high selectivity (70%) for C2 products of GB-Cu at –1.0 V *vs.* RHE, a 6-cell a-Si/c-Si heterojunction (SHJ) module is adopted (Figure S14, details in Supporting Information) to couple with the flow cell directly. The operation point determined by the intersection of two LSV curves is very close to the maximum power point (MPP) of the solar cell module (Figure 4c), meaning that two devices can match well with each other. Meanwhile, a higher current density could be reached in the flow cell compared with the traditional H-cell, where a stable current density of 52.1 mA·cm^{-2} (Figure 4d) is obtained at a voltage of ~2.8 V in EC cell (Figure S15) without external bias under AM 1.5G illumination. The FE of C2 products reaches up to 68 % during the 3h operation. According to the operating current and FE of C2 products, the solar-to-C2-products efficiency achieves 3.88% (details in Supporting Information). Few PV-EC devices can convert solar energy into chemical energy in C2 products under such a large current density and high efficiency (Table S4).

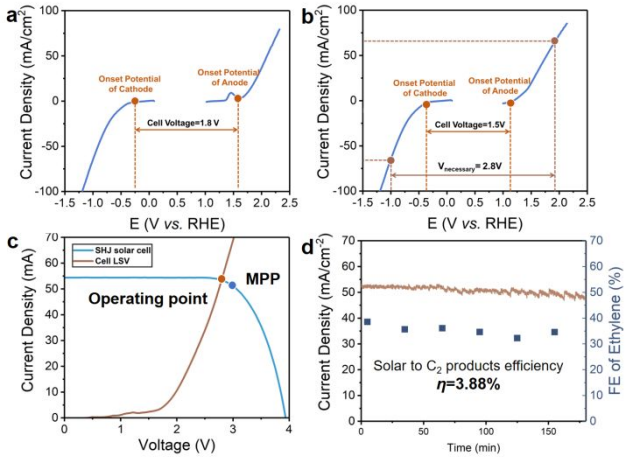

Figure 4. (a) LSV of GB-Cu cathode and Ni foam anode; (b) LSV of GB-Cu cathode and Se-(NiCo)S_x/$(OH)_x$ anode; (c) Current–potential characteristic of the SHJ solar cell under 1 sun (AM 1.5G) illumination (blue line) and measured operating current of the electrolyzer cell (brown line); (d) The stability test of PV-EC device.

In summary, GBs are introduced into metallic copper in a facile approach in which PVP is applied as the additive. Compared with normal copper electrocatalyst, GB-Cu exhibits a high selectivity (FE =~70%) to C2 products in a wide potential range of –1.0 to –1.3 V *vs.* RHE. In-situ ATR-SEIRAS and DFT reveal that the existence of GBs on metallic copper enhances the adsorption of key intermediate (*CO) to promote the C–C coupling reaction. Subsequently, a low-cost PV-EC system with all-earth-abundant materials is designed to convert CO_2 into C2 products at a remarkable solar-to-fuel conversion of 3.88%. This grain-boundary-rich copper electrocatalyst and its use in the PV-EC device show new possibilities in applications for the solar-driven CO_2 reaction.

ASSOCIATED CONTENT

Supporting Information

Experimental details and supporting data. This material is available free of charge via the Internet at http://pubs.acs.org.

AUTHOR INFORMATION

Corresponding Author

*Email: jlgong@tju.edu.cn

ORCID

Jinlong Gong: 0000-0001-7263-318X
Tuo Wang: 0000-0002-9862-5038

Zhi-Jian Zhao: 0000-0002-8856-5078

Notes

The authors declare no competing financial interests.

ACKNOWLEDGMENT

We acknowledge the National Key R&D Program of China (2016YFB0600901), the National Natural Science Foundation of China (21525626, U1662111, 21722608, 51861125104), the Natural Science Foundation of Tianjin City (18JCJQJC47500) and the Program of Introducing Talents of Discipline to Universities (B06006) for financial support.

REFERENCES

(1) Bushuyev, O. S.; De Luna, P.; Dinh, C. T.; Tao, L.; Saur, G.; van de Lagemaat, J.; Kelley, S. O.; Sargent, E. H., What Should We Make with CO_2 and How Can We Make It? *Joule* **2018,** *2*, 825-832.

(2) Huan, T. N.; Dalla Corte, D. A.; Lamaison, S.; Karapinar, D.; Lutz, L.; Menguy, N.; Foldyna, M.; Turren-Cruz, S. H.; Hagfeldt, A.; Bella, F.; Fontecave, M.; Mougel, V., Low-Cost High-Efficiency System for Solar-Driven Conversion of CO_2 to Hydrocarbons. *Proc. Natl. Acad. Sci.U. S. A.* **2019,** *116*, 9735-9740.

(3) Vasileff, A.; Xu, C.; Jiao, Y.; Zheng, Y.; Qiao, S.-Z., Surface and Interface Engineering in Copper-Based Bimetallic Materials for Selective CO_2 Electroreduction. *Chem* **2018,** *4*, 1809-1831.

(4) Bagger, A.; Ju, W.; Varela, A. S.; Strasser, P.; Rossmeisl, J., Electrochemical CO_2 Reduction: A Classification Problem. *Chemphyschem* **2017,** *18*, 3266-3273.

(5) Morales-Guio, C. G.; Cave, E. R.; Nitopi, S. A.; Feaster, J. T.; Wang, L.; Kuhl, K. P.; Jackson, A.; Johnson, N. C.; Abram, D. N.; Hatsukade, T.; Hahn, C.; Jaramillo, T. F., Improved CO_2 Reduction Activity towards C2+ Alcohols on a Tandem Gold on Copper Electrocatalyst. *Nat. Catal.* **2018,** *1*, 764-771.

(6) Scholten, F.; Sinev, I.; Bernal, M.; Roldan Cuenya, B., Plasma-Modified Dendritic Cu Catalyst for CO_2 Electroreduction. *ACS Catal* **2019,** *9*, 5496-5502.

(7) Kuhl, K. P.; Cave, E. R.; Abram, D. N.; Jaramillo, T. F., New Insights into the Electrochemical Reduction of Carbon Dioxide on Metallic Copper Surfaces. *Energy Environ. Sci.* **2012,** *5*, 7050-7059.

(8) Feng, X.; Jiang, K.; Fan, S.; Kanan, M. W., Grain-Boundary-Dependent CO_2 Electroreduction Activity. *J. Am. Chem. Soc.* **2015,** *137*, 4606-4609.

(9) Liu, S.; Xiao, J.; Lu, X. F.; Wang, J.; Wang, X.; Lou, X. W. D., Efficient Electrochemical Reduction of CO_2 to HCOOH over Sub-2 nm SnO_2 Quantum Wires with Exposed Grain Boundaries. *Angew. Chem. Int. Ed.* **2019,** *58*, 8499-8503.

(10) Feng, X.; Jiang, K.; Fan, S.; Kanan, M. W., A Direct Grain-Boundary-Activity Correlation for CO Electroreduction on Cu Nanoparticles. *ACS Cent. Sci.* **2016,** *2*, 169-174.

(11) Verdaguer-Casadevall, A.; Li, C. W.; Johansson, T. P.; Scott, S. B.; McKeown, J. T.; Kumar, M.; Stephens, I. E.; Kanan, M. W.; Chorkendorff, I., Probing the Active Surface Sites for CO Reduction on Oxide-Derived Copper Electrocatalysts. *J. Am. Chem. Soc.* **2015,** *137*, 9808-9811.

(12) Ren, D.; Deng, Y. L.; Handoko, A. D.; Chen, C. S.; Malkhandi, S.; Yeo, B. S., Selective Electrochemical Reduction of Carbon Dioxide to Ethylene and Ethanol on Copper(I) Oxide Catalysts. *ACS Catal.* **2015,** *5*, 2814-2821.

(13) Li, C. W.; Ciston, J.; Kanan, M. W., Electroreduction of Carbon Monoxide to Liquid Fuel on Oxide-Derived Nanocrystalline Copper. *Nature* **2014,** *508*, 504-507.

(14) Kim, J.; Choi, W.; Park, J. W.; Kim, C.; Kim, M.; Song, H., Branched Copper Oxide Nanoparticles Induce Highly Selective Ethylene Production by Electrochemical Carbon Dioxide Reduction. *J. Am. Chem. Soc.* **2019,** *141*, 6986-6994.

(15) Chen, Z.; Chang, J. W.; Balasanthiran, C.; Milner, S. T.; Rioux, R. M., Anisotropic Growth of Silver Nanoparticles is Kinetically Controlled by Polyvinylpyrrolidone Binding. *J. Am. Chem. Soc.* **2019,** *141*, 4328-4337.

(16) Granata, G.; Yamaoka, T.; Pagnanelli, F.; Fuwa, A., Study of the Synthesis of Copper Nanoparticles: the Role of Capping and Kinetic towards Control of Particle Size and Stability. *J. Nanopart. Res.* **2016,** *18*, 133.

(17) Koczkur, K. M.; Mourdikoudis, S.; Polavarapu, L.; Skrabalak, S. E., Polyvinylpyrrolidone (PVP) in Nanoparticle Synthesis. *Dalton Trans.* **2015,** *44*, 17883-17905.

(18) Hempelmann, H. N. R., Nanocrystalline Copper by Pulsed Electrodeposition: The Effects of Organic Additives, Bath Temperature, and pH. *J. Phys. Chem.* **1996,** *100*, 19525-19532.

(19) Jung, H.; Lee, S. Y.; Lee, C. W.; Cho, M. K.; Won, D. H.; Kim, C.; Oh, H. S.; Min, B. K.; Hwang, Y. J., Electrochemical Fragmentation of Cu_2O Nanoparticles Enhancing Selective C–C Coupling from CO_2 Reduction Reaction. *J. Am. Chem. Soc.* **2019,** *141*, 4624-4633.

(20) Grosse, P.; Gao, D.; Scholten, F.; Sinev, I.; Mistry, H.; Roldan Cuenya, B., Dynamic Changes in the Structure, Chemical State and Catalytic Selectivity of Cu Nanocubes during CO_2 Electroreduction: Size and Support Effects. *Angew. Chem. Int. Ed.* **2018,** *57*, 6192-6197.

(21) Zhuang, T. T.; Pang, Y. J.; Liang, Z. Q.; Wang, Z. Y.; Li, Y.; Tan, C. S.; Li, J.; Dinh, C. T.; De Luna, P.; Hsieh, P. L.; Burdyny, T.; Li, H. H.; Liu, M. X.; Wang, Y. H.; Li, F. W.; Proppe, A.; Johnston, A.; Nam, D. H.; Wu, Z. Y.; Zheng, Y. R.; Ip, A. H.; Tan, H. R.; Chen, L. J.; Yu, S. H.; Kelley, S. O.; Sinton, D.; Sargent, E. H., Copper Nanocavities Confine Intermediates for Efficient Electrosynthesis of C3 Alcohol Fuels from Carbon Monoxide. *Nat. Catal.* **2018,** *1*, 946-951.

(22) Lum, Y.; Ager, J. W., Evidence for Product-Specific Active Sites on Oxide-Derived Cu Catalysts for Electrochemical CO_2 Reduction. *Nat. Catal.* **2018,** *2*, 86-93.

(23) Hahn, C.; Hatsukade, T.; Kim, Y. G.; Vailionis, A.; Baricuatro, J. H.; Higgins, D. C.; Nitopi, S. A.; Soriaga, M. P.; Jaramillo, T. F., Engineering Cu Surfaces for the Electrocatalytic Conversion of CO_2: Controlling Selectivity toward Oxygenates and Hydrocarbons. *Proc. Natl. Acad. Sci.U. S. A.* **2017,** *114*, 5918-5923.

(24) Karimzadeh, I.; Aghazadeh, M.; Ganjali, M. R.; Norouzi, P.; Shirvani-Arani, S.; Doroudi, T.; Kolivand, P. H.; Marashi, S. A.; Gharailou, D., A Novel Method for Preparation of Bare and Poly(vinylpyrrolidone) Coated Superparamagnetic Iron Oxide Nanoparticles for Biomedical Applications. *Mater. Lett.* **2016,** *179*, 5-8.

(25) Arihara, K.; Kitamura, F.; Ohsaka, T.; Tokuda, K., Characterization of the Adsorption State of Carbonate Ions at the Au(111) Electrode Surface using In Situ IRAS. *J. Electroanal. Chem.* **2001,** *510*, 128-135.

(26) Heyes, J.; Dunwell, M.; Xu, B., CO_2 Reduction on Cu at Low Overpotentials with Surface-Enhanced in Situ Spectroscopy. *J. Phys. Chem. C* **2016,** *120*, 17334-17341.

(27) Gunathunge, C. M.; Ovalle, V. J.; Li, Y. W.; Janik, M. J.; Waegele, M. M., Existence of an Electrochemically Inert CO Population on Cu Electrodes in Alkaline pH. *ACS Catal.* **2018,** *8*, 7507-7516.

(28) Malkani, A. S.; Dunwell, M.; Xu, B., Operando Spectroscopic Investigations of Copper and Oxide-Derived Copper Catalysts for Electrochemical CO Reduction. *ACS Catal.* **2018,** *9*, 474-478.

(29) Lee, S.; Lee, J., Ethylene Selectivity in CO Electroreduction when using Cu Oxides: An In Situ ATR-SEIRAS Study. *ChemElectroChem* **2018,** *5*, 558-564.

(30) Zhu, S. Q.; Li, T. H.; Cai, W. B.; Shao, M. H., CO_2 Electrochemical Reduction as Probed through Infrared Spectroscopy. *ACS Energy Lett.* **2019,** *4*, 682-689.

(31) Gunathunge, C. M.; Ovalle, V. J.; Waegele, M. M., Probing Promoting Effects of Alkali Cations on the Reduction of CO at the Aqueous Electrolyte/Copper Interface. *Phys. Chem. Chem. Phys.* **2017,** *19*, 30166-30172.

(32) Persson, B. N. J.; Ryberg, R., Vibrational Interaction between Molecules Adsorbed on a Metal Surface: The Dipole-Dipole Interaction. *Phys. Rev. B* **1981,** *24*, 6954-6970.

(33) Gunathunge, C. M.; Li, X.; Li, J. Y.; Hicks, R. P.; Ovalle, V. J.; Waegele, M. M., Spectroscopic Observation of Reversible Surface Reconstruction of Copper Electrodes under CO_2 Reduction. *J. Phys. Chem. C* **2017,** *121*, 12337-12344.

(34) Kim, K. S.; Kim, W. J.; Lim, H. K.; Lee, E. K.; Kim, H., Tuned Chemical Bonding Ability of Au at Grain Boundaries for Enhanced Electrochemical CO_2 Reduction. *ACS Catal.* **2016,** *6*, 4443-4448.

(35) Goodpaster, J. D.; Bell, A. T.; Head-Gordon, M., Identification of Possible Pathways for C–C Bond Formation during Electrochemical Reduction of CO_2: New Theoretical Insights from an Improved Electrochemical Model. *J. Phys. Chem. Lett.* **2016,** *7*, 1471-1477.

(36) Calle-Vallejo, F.; Koper, M. T., Theoretical Considerations on the Electroreduction of CO to C2 species on Cu(100) electrodes. *Angew. Chem. Int. Ed.* **2013,** *52*, 7282-7285.

(37) Jiang, K.; Sandberg, R. B.; Akey, A. J.; Liu, X.; Bell, D. C.; Nørskov, J. K.; Chan, K.; Wang, H., Metal Ion Cycling of Cu Foil for Selective C–C Coupling in Electrochemical CO_2 Reduction. *Nat. Catal.* **2018,** *1*, 111-119.
(38) Garza, A. J.; Bell, A. T.; Head-Gordon, M., Mechanism of CO_2 Reduction at Copper Surfaces: Pathways to C2 Products. *ACS Catal.* **2018,** *8*, 1490-1499.
(39) Bertheussen, E.; Verdaguer-Casadevall, A.; Ravasio, D.; Montoya, J. H.; Trimarco, D. B.; Roy, C.; Meier, S.; Wendland, J.; Norskov, J. K.; Stephens, I. E.; Chorkendorff, I., Acetaldehyde as an Intermediate in the Electroreduction of Carbon Monoxide to Ethanol on Oxide-Derived Copper. *Angew. Chem. Int. Ed.* **2016,** *55*, 1450-1454.
(40) Hu, C.; Zhang, L.; Zhao, Z. J.; Li, A.; Chang, X.; Gong, J., Synergism of Geometric Construction and Electronic Regulation: 3D Se-$(NiCo)S_x/(OH)_x$ Nanosheets for Highly Efficient Overall Water Splitting. *Adv. Mater.* **2018,** *30*, e1705538.

Table of Contents